

Impact of medium effects on the cooling of non–superfluid and superfluid neutron stars

Ch. Schaab¹, D. Voskresensky^{2,3}, A. D. Sedrakian⁴, F. Weber^{1,5}, and M. K. Weigel¹

¹Institute for Theoretical Physics, Ludwig-Maximilians Universität, Theresienstrasse 37/III, D-80333 Munich, Germany

²Gesellschaft für Schwerionenforschung GSI, P. O. Box 110552, D-64220 Darmstadt, Germany

³Moscow Institute for Physics and Engineering, 115409 Moscow, Kashirskoe shosse 31, Russia

⁴Max-Planck-Society, Research unit 'Theoretical Many-Particle Physics' at Rostock University, Universitätplatz 1, D-18051 Rostock, Germany

⁵Nuclear Science Division, Lawrence Berkeley National Laboratory, MS: 70A-3307, University of California, Berkeley, CA 94720, USA

Received; accepted

Abstract. Neutrino emission from the dense hadronic component in neutron stars is subject to strong modifications due to collective effects in the nuclear medium. We implement new estimates of the neutrino emissivities of two processes operating in the nuclear medium into numerical cooling simulations of neutron stars. The first process is the modified Urca process, for which the softening of the pion exchange mode and other polarization effects as well as the neutrino emission arising from the intermediate reaction states are taken into account. The second process concerns neutrino emission through superfluid pair breaking and formation processes. It is found that the medium effects on the emissivity of the modified Urca process result in a strong density dependence, which gives a smooth crossover from the standard

Send offprint requests to: Ch. Schaab, email: schaab@gsm.sue.physik.uni-muenchen.de

to the nonstandard cooling scenario for increasing star masses. For superfluid stars, the superfluid pair breaking and formation processes accelerate mildly both the standard and the nonstandard cooling scenario. This leads to a good agreement between the theoretical cooling tracks and the rather low temperatures observed for objects like PSRs 0833-45 (Vela), 0656+14, and 0630+18 (Geminga). The robustness of our findings against variations in both the underlying equation of state of baryonic matter and the used fast cooling processes is demonstrated. Hence we conclude that the two recalculated neutrino emissivities studied here enable one to reproduce theoretically most of the observed pulsar temperatures by varying the masses of neutron star models.

Key words: Stars: neutron – Stars: evolution – Dense matter – X-rays: stars

1. Introduction

The physics of neutron star cooling is based on a number of ingredients, among which the neutrino emissivity of the high-density hadronic matter in the star's core plays an important role. Depending on the dominant neutrino-emission process at the early stages of the thermal evolution, the cooling simulations follow either the slow (standard) or the fast (nonstandard) scenario of thermal evolution. In the first case the dominant neutrino-radiation reactions are the modified Urca and the bremsstrahlung processes. In the second case, these are the pion (kaon) β -decay processes, direct Urca on nucleons and hyperons, as well as their analogous reactions taking place in the deconfined quark phase. The main difference in the cooling efficiency driven by these processes lies in the rather different phase spaces associated with these reactions. In the first case the available phase space is that of a two-baryon scattering process, while in the second case it is that of a one-baryon decay process.

Numerical simulations of neutron star cooling, incorporating these types of neutrino emission, have been extensively performed in the past (see, for instance, Tsunura 1966, Richardson et al. 1982, Van Riper 1991, and Schaab et al. 1996a). These calculations suggest that the combined soft X-ray data from Einstein, EXOSAT, and ROSAT are roughly consistent with the slow cooling scenario, depending on the equation of state and the uncertainties associated with the behavior of superdense matter. Some pulsars, however, as for example Vela and Geminga, possess rather low temperatures and thus seem to call for a more rapid cooling than is

obtained for the modified Urca process. The fast cooling scenarios, on the other hand, generally have the tendency to underestimate the surface temperatures of these pulsars. So a natural question, motivated by these observations, is whether the physics of neutrino emission from the star's dense core will be able to resolve this problem. This will be discussed in this paper. Obviously, the corresponding modifications must be such that the theoretical cooling curves describe both the hotter as well as cooler classes of pulsars, which could be linked to variations in gross-structure parameters, like the star's mass (Voskresensky & Senatorov 1984 (VS84), 1986 (VS86)).

The aim of the present work is to implement a number of medium-modified neutrino emissivities, which dominate a neutron star's thermal evolution, in numerical cooling simulations of such objects. We shall demonstrate that by means of this one is indeed able to achieve agreement with both the high as well as low observed pulsar temperatures.

It is a well established fact that neutrino emission at the early stages of the standard evolution is dominated by the modified Urca and bremsstrahlung processes. The neutrino radiation in the modified Urca process was first estimated by Bahcall & Wolf (1965) and by Tsuruta & Cameron (1965). Bremsstrahlung processes dealing with the neutral currents were first evaluated by Flowers et al. (1975). Then the corresponding rates have been more closely studied by Friman & Maxwell (1979,FM79) resulting in sufficiently higher rates. The calculation were performed in the free one-pion-exchange approximation to the long-range part of the nucleon-nucleon (NN) interaction, supplemented by a parametrization of the short-range part of the NN interaction by the Landau Fermi-liquid parameters. Medium effects enter these rates mainly through the effective mass of the nucleons. Therefore the density dependence of the rates is rather weak and the neutrino radiation from a neutron star depends only very weakly on its mass. This is the reason why the standard scenario based on the FM79 result, though complying well with a few slowly cooling pulsars, fails to explain the data of the more rapidly cooling ones.

Here, we shall carry out detailed simulations of the cooling of neutron star models, which incorporate the softening of the one-pion exchange mode, other medium polarization effects, like the inclusion of the nucleon-nucleon correlations in the vertices, as well as the possibility of neutrino emission from intermediate reaction states¹ (VS84, VS86). We also include the processes of neutrino pair radiation

¹ E.g., the pion participating in the exchange between the nucleons may also radiate the neutrinos or decay in intermediate reaction states to the nucleon-nucleon hole with

from superfluid nucleon pair breaking and formation mechanism first estimated by Flowers et al. (1976), and then more closely studied by Voskresensky & Senatorov (1987) and Senatorov & Voskresensky (1987) using the closed diagram technique. The medium modifications of these rates result in a pronounced density dependence, which, in turn, links the cooling behavior of a neutron star decisively to its mass.

Using a collection of modern equations of state for nuclear matter in its ground state, which covers both relativistic as well as non-relativistic models, we shall demonstrate the robustness of the new cooling mechanisms against variations in the equation of state of super-dense neutron star matter. Part of these variations are caused by the possible superfluid behavior of neutron star matter. To demonstrate this effect on the new cooling mechanisms, we proceed in three successive steps, starting from stars made up of non-superfluid matter. These models are then supplemented with superfluidity, with superfluid gap parameters taken from the literature. Unfortunately, the gap energies are not very well known because of uncertainties in the effective baryon masses, the nucleon–nucleon interaction, and polarization effects (cf. Chen et al. 1993). To account for these uncertainties, their values are finally varied about the theoretically determined ones. Since there are also uncertainties concerning the possibility of fast cooling processes the calculations are done with both the nucleon direct Urca and the β -decay processes in pion condensates (pion Urca) and additionally without any fast cooling process.

We shall show that the above mentioned medium–modifications lead to a more rapid cooling than obtained for the standard scenario. Hence they provide a possible explanation for the observed deviations of some of the pulsar temperatures from standard cooling. Particularly, it is shown that they provide a smooth transition from standard to nonstandard cooling for increasing central star densities, i.e., star masses.

The paper is organized as follows. In Sect. 2 we briefly discuss the incorporated neutrino emission processes which comprise the modified Urca, superfluid nucleon–pair breaking and formation, direct Urca and pion Urca processes. In Sect. 3 the neutron star cooling simulations and the physical input quantities used in the calculations are described. In Sect. 4 we present the results of the numerical calculations and compare them with the observed data. The conclusions are summarized in the last section.

subsequent neutrino radiation. This essentially modifies the absolute value as well as the density dependence of the modified Urca process rate.

2. Neutrino Emissivities

2.1. Medium Effects on the Modified Urca Process

The modified Urca (MU^2) process is linked to neutrino emission via a weak decay of a nucleon in the presence of a bystander nucleon. The latter ensures that both momentum and energy are conserved in the reaction. The two topologically different diagrams contributing to these processes are schematically shown in Fig. 1. The first diagram shows the neutrino radiation from a nucleon “leg”, i.e., from an initial- or final-state nucleon. The shaded block represents the total nucleon-nucleon interaction amplitude in the medium (including the softening of the pion mode, corrections of the vertices by the nucleon-nucleon-hole and delta-nucleon-hole loops, and modifications of the short-range interaction by nucleon-nucleon-hole and delta-nucleon-hole loops), while the filled circle stands for the nucleon-nucleon correlations. The second diagram illustrates the neutrino radiation from the intermediate scattering states (like neutrino radiation by the pion and the nucleon-nucleon hole loop being present in intermediate reaction states). Such medium effects as well as the second reaction channel were not incorporated in the calculations by FM79 and shall lead to a rather new cooling behavior, as we will see below.

Table 1. Key to abbreviations

abbreviation	meaning
MU-FM79	modified Urca process calculated by FM79
MU-VS86	modified Urca process calculated by VS86
NPBF	neutron pair-breaking and formation
PPBF	proton pair-breaking and formation
DU	direct Urca process
PU	pion Urca process

The main contribution to the nucleon-nucleon interaction amplitude at densities $n \gtrsim 0.5-0.7 n_0$, where $n_0 \simeq 0.16 \text{ fm}^{-3}$ is the nuclear matter saturation density, is determined by the in-medium one-pion-exchange supplemented by medium-modified

² We shall abbreviate the modified Urca process calculated via the free one-pion exchange model by Friman and Maxwell with MU-FM79. The abbreviation MU-VS86 will refer to the process which accounts for the additional included medium modification effects. The abbreviations of the various neutrino-emitting processes considered in this paper are summarized in Table 1.

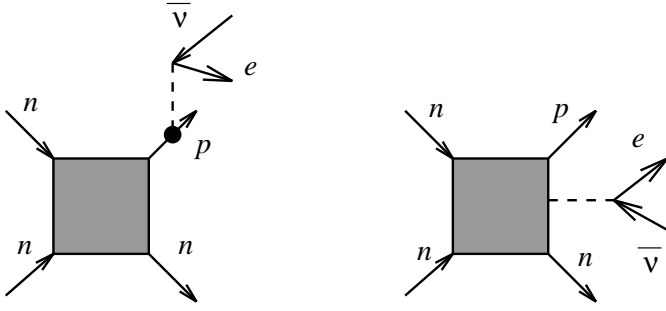


Fig. 1. Neutrino emission from a nucleon leg (left graph) and from intermediate scattering states (right graph). Details are given in the text.

vertices (VS86), whereas the peculiarities of a more local part of the interaction play an important part only at rather small densities, $n \lesssim 0.5n_0$ (Blaschke et al. 1995). At $n \gtrsim n_0$ the emissivity arising from the modified Urca is dominated by the second diagram of Fig. 1, whereas the first diagram gives only small corrections (VS86, Voskresensky et al. 1987, Haubold et al. 1988). The contributions of the first diagram, which gives the only contribution to emissivity calculated by FM79, can therefore be neglected. The resulting emissivity reads in a simplified notation as follows (VS86, Migdal et al. 1990),

$$\begin{aligned} \epsilon_\nu^{(\text{MU-VS86})} &\simeq 2.4 \times 10^{24} F_1 \left(\frac{n}{n_0}\right)^{10/3} \left(\frac{m_N^*(n)}{m_N}\right)^4 \\ &\times \left[\frac{m_\pi}{\alpha \tilde{\omega}[p_{Fn}(n)]}\right]^8 \Gamma^8 T_9^8 \\ &\times \zeta(\Delta_n) \zeta(\Delta_p) \frac{\text{erg}}{\text{cm}^3 \text{sec}}, \end{aligned} \quad (1)$$

where $T_9 = T/10^9 K$ is the temperature, m_N^* and m_N are the effective and bare nucleon mass, respectively, $p_{Fn}(n)$ is the density dependent neutron Fermi-momentum, and the factor

$$F_1 = 1 + \frac{3}{4\Gamma^2} \left(\frac{n}{n_0}\right)^{2/3}$$

is the correction due to the pion decay from intermediate states. It reduces to unity when the intermediate state pion decay processes are ignored and only contributions from the weak current decay in the nucleon-nucleon-hole being present in intermediate reaction states are taken into account.

The quantity Γ accounts for the nucleon-nucleon correlations in the πNN vertices. The effective pion gap, $\tilde{\omega}^2$, expressed in units of $m_\pi = 140$ MeV, is given by $\tilde{\omega}[p_{Fn}(n)] \simeq -D_\pi^{-1}(\omega \simeq \mu_\pi, k = p_{Fn}(n))$, where D_π^{-1} is the in-medium pion Green

function, μ_π is the pion chemical potential. (For simplicity, we set the chemical potentials of π^+ , π^- , and π^0 mesons equal to $\mu_\pi \simeq 0$.)

The values of $\tilde{\omega}^2$ and Γ for isospin symmetric nuclear matter at saturation density are extracted from the atomic nuclei data. For the case of interest, $\mu_\pi = 0$, they read $\Gamma(n_0) \simeq 0.4$ and $\tilde{\omega}^2(n_0) \simeq 0.8 - 0.95$ (Migdal et al. 1990). For highly asymmetric nuclear matter, especially for $n > n_0$, the magnitude and density dependence of $\tilde{\omega}^2(n)$ and $\Gamma(n)$ are not well known. In the present calculations we approximate the form-factor in the effective πNN vertex, $\Gamma(n)$, by the formula

$$\Gamma(n) \approx \frac{1}{1 + 1.4(n/n_0)^{1/3}}, \quad (2)$$

which shows the explicit functional dependence on the density.³ The effective pion gap $\tilde{\omega}^2(n)$ has been estimated in Migdal (1978), Voskresensky & Mishustin (1978, 1982), and Migdal et al. (1990) for different parameter choices. We apply two different parametrizations in the cooling calculations (see Fig. 2). The first one assumes a phase transition into the pion condensate phase at $n_c = 3n_0$ (Brown & Weise 1976, Migdal 1978, Migdal et al. 1990), while the second one assumes that there is no phase transition (for a more detailed discussion see Sect. 2.3). Due to the pion-fluctuation effect the pion condensation sets in via a first order phase transition (see Dyugaev 1975, Voskresensky & Mishustin 1978, 1982). This manifests itself in a jump of the pion gap at $n = n_c^\pi$ from a positive value to a negative one, see solid line in Fig 2.⁴ It has to be emphasized that the density dependence of $\tilde{\omega}^2(n)$ is rather unknown. Our choices for the parametrization are motivated by microscopic many-body calculations. Somewhat different choices for the values of $\tilde{\omega}^2(n)$, $\Gamma(n)$ and the critical density for the onset of pion condensation affect of course the resulting cooling rates. The qualitative conclusions, however, remain unchanged. Indeed, as we will see below, the cooling curves for the two different parametrizations of $\tilde{\omega}^2(n)$ do not differ very much (see e.g. Fig. 8).

The value of the parameter α is given by $\alpha = 1$ for $n < n_c^\pi$, and $\alpha = \sqrt{2}$ for $n > n_c^\pi$. This parameter accounts for the changes caused by the neutrino emissivity of the modified Urca process below and above the critical point where pion condensation occurs (cf. VS86).

³ This implies in our case that the Landau-Migdal parameter g' scales as $(n/n_0)^{1/3}$ leading to an increasing repulsion for higher densities.

⁴ Without this behavior one would get an anomalous increase of the neutrino emissivity via bremsstrahlung in the vicinity of the critical point. This effect is analogous to the critical opalescence phenomenon (VS86).

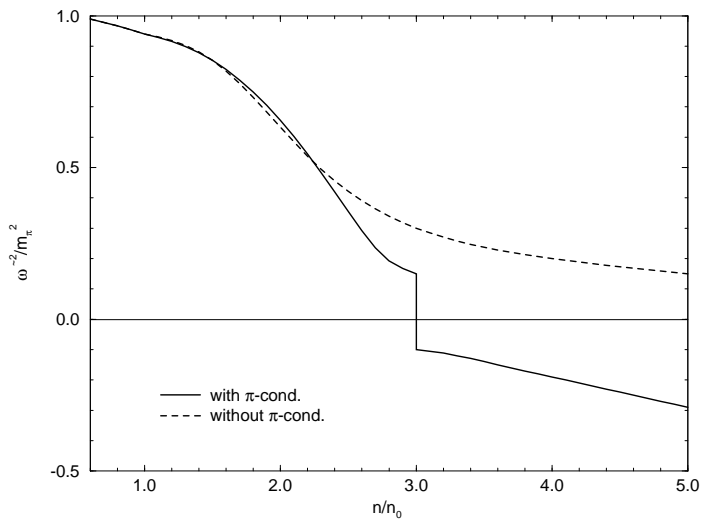


Fig. 2. Effective pion gap $\tilde{\omega}^2/m_\pi^2$ versus density with (solid line) and without pion condensation (dashed line). $n_0 = 0.16 \text{ fm}^{-3}$ denotes the nuclear saturation density.

The factor

$$\zeta(\Delta_n) = \begin{cases} \exp(-\Delta_n/k_B T) & T \leq T_{cn}, \\ 1 & T > T_{cn} \end{cases} \quad (3)$$

takes roughly into account the suppression caused by the nucleon pairing, where Δ_n and T_{cn} are the superfluid gap and the critical temperature for superfluid phase transition of neutrons. The factor $\zeta(\Delta_p)$ is defined in the analogous way and takes into account the proton–proton pairing.

2.2. Cooper Pair–Breaking and Pair–Formation Processes

When a neutron star cools down to temperatures in the vicinity of the critical temperature for pairing of neutrons and protons, pairing correlations play an increasingly important role in the dynamics of the star’s thermal evolution. Generally, the onset of superfluidity tends to slow down the cooling rate of a neutron star, since the neutrino emission processes are drastically suppressed. It enables however two additional processes as noticed in Flowers et al. (1976) and Voskresensky & Senatorov (1987): the superfluid neutron–pair breaking and formation process (NPBF) and the superfluid proton–pair breaking and formation process (PPBF).

The superfluid in a neutron star can be considered as a two–component system, which, for a fixed density and temperature, consists of paired quasiparticles in the condensate and elementary excitations above the condensate. Their associated quasi–equilibrium densities are controlled by Cooper–pair–formation and pair–breaking processes. These processes, which are rather frequent at temperatures in

the vicinity of T_c , become successively suppressed at lower temperatures, because of an exponential increase in the number of paired particles. As shown in Fig. 3, these processes proceed with the emission of neutrino pairs via the reactions $\{NN\} \rightarrow N + N + \nu + \bar{\nu}$ and $N + N \rightarrow \{NN\} + \nu + \bar{\nu}$, where $\{NN\}$ denotes the Cooper pair, N an excitation.

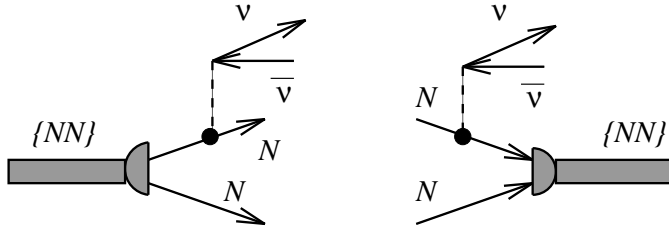


Fig. 3. Neutrino emission from Cooper pair-breaking (left graph) and pair-formation processes (right graph). Details are given in the text.

The respective emission rates can be calculated either in terms of the closed diagram formalism, using the normal and anomalous Green's functions for the paired nucleons, or in terms of the method of Bogoliubov's transformations applied to reaction rates in the normal ground state. As far as one works in the quasiparticle limit, which is an excellent approximation for neutron star matter, the preference for one or the other method is primarily a matter of taste. However, in a broader context, the Green's functions method provides a more general treatment by allowing for off-mass-shell effects and a systematic diagrammatical representation of the approximations to the self-energy functions (scattering rates). A first estimate of the reaction rates was given by Flowers et al. (1976) using the Bogoliubov's transformations. It was recalculated by Voskresensky & Senatorov (1987) using closed diagram technique. Voskresensky & Senatorov have also included the contribution of the axial vector coupling and used different parameterizations of the weak coupling vertices. This results in a rate being higher by an order of magnitude. Besides the NPBF process, the PPBF process was considered, too. One finds in lowest order of the expansion parameters T/ϵ_{Fn} and T/ϵ_{Fp} (ϵ_{Fn} and ϵ_{Fp} are the Fermi-energies of neutrons and protons, respectively) for the neutron and proton components (see Voskresensky & Senatorov 1987)

$$\begin{aligned} \epsilon_{\nu}^{(NPBF)} &\simeq 6.6 \times 10^{28} \left(\frac{n}{n_0}\right)^{1/3} \frac{m_N^*}{m_N} \left(\frac{\Delta_n}{\text{MeV}}\right)^7 \\ &\times I\left(\frac{\Delta_n}{T}\right) \quad \text{for } T < T_c^n, \end{aligned} \quad (4)$$

$$\epsilon_{\nu}^{(PPBF)} \simeq 1.7 \times 10^{28} \left(\frac{n}{n_0}\right)^{1/3} \frac{m_N^*}{m_N} \left(\frac{\Delta_p}{\text{MeV}}\right)^7 \times I\left(\frac{\Delta_p}{T}\right) \quad \text{for } T < T_c^p, \quad (5)$$

where

$$I(x) = \int_0^{\infty} \frac{(\text{ch}y)^5 dy}{[\exp(x\text{ch}y) + 1]^2} \simeq e^{-2x} \sqrt{\pi/4x} \quad \text{for } x = \Delta/T \gg 1. \quad (6)$$

It can be seen that in the limit $\Delta/T \gg 1$, the rate of these processes is exponentially suppressed, as it is the case for the two-nucleon process considered above. However, because of mild phase space restrictions (we deal here effectively with a one-nucleon phase-space volume) these processes may considerably contribute to the neutrino emissivity of the neutron star. The maximum value of $(\Delta(T)/\Delta(T=0))^7 I(\Delta(T)/T)$ depends only on the ratio $\Delta(T=0)/T_c$. For $^1\text{S}_0$ -pairing the maximum value is equal to $\approx 10^{-2}$, for $^3\text{P}_2$ -pairing it is $\approx 10^{-6}$. This causes the emissivity of the NPBF process in the core ($^3\text{P}_2$ -pairing) to be smaller by three orders of magnitude (for equal gap energies) compared to the emissivity in the crust ($^1\text{S}_0$ -pairing).

2.3. Direct Urca Process and Pion Urca Process

Along with the two processes described above we include in the numerical calculations other relevant channels of neutrino emission, too. Though we shall see that the processes described above lead to “*intermediate*” cooling rates, it still appears useful to distinguish between “*standard cooling*” and “*nonstandard*” or “*fast cooling*”, depending on whether the predominant process is the modified Urca process or a faster one, as nucleon or hyperon direct Urca, processes in pion- or kaon-condensed matter, or those caused by the presence of quarks in dense matter.

As examples of a fast cooling processes, we shall use the nucleon direct Urca (DU) and the pion Urca (PU) processes. These processes are rather representative for other fast processes. Indeed, all the fast cooling processes lead qualitatively to the same temperature dependence of the emissivity, $\sim T^6$. Moreover the values of the critical densities beyond which these processes are possible are close to each other.

The DU processes

$$n \rightarrow p + e^- + \bar{\nu}_e \quad \text{and} \quad p + e^- \rightarrow n + \nu_e \quad (7)$$

can only occur if the proton fraction exceeds some critical value (about 11–13 % depending on the composition) in order to fulfill energy and momentum conservation (see Boguta 1981 and Lattimer et al. 1991). In contrast to nonrelativistic EOS's (e.g. UV₁₄+UVII) which predict proton fractions that lie below these critical values, relativistic EOS's contain sufficiently large proton fractions such that the direct Urca process becomes possible. However, the proton fraction depends crucially on the symmetry energy which is unfortunately not well known at higher densities. We shall use the emissivity calculated by Lattimer et al. (1991), however corrected by the suppression factor Γ^2 (see eq. (2)) accounting for the nucleon–nucleon correlations in the weak interaction vertex (for simplicity, we assume the same suppression factor in all vertices, cf. discussion in Voskresensky & Senatorov 1987):

$$\epsilon_{\nu}^{(\text{DU})} \simeq 4 \times 10^{27} \left(\frac{n_e}{n_0} \right)^{1/3} \left(\frac{m_N^*}{m_N} \right)^2 \Gamma^2 T_9^6 \zeta(\Delta_n) \zeta(\Delta_p) \frac{\text{erg}}{\text{cm}^3 \text{ sec}} . \quad (8)$$

The impact of the direct Urca process on the cooling will be shown in Sect. 4.4, where the final results are discussed, whereas it is neglected in the other cooling curves in order to demonstrate the efficiency of MU-VS86 and NPBF and PPBF-processes.

Even more uncertain is the possibility of the hyperon direct Urca (see Prakash et al. 1992). Whereas the contribution of the hyperon direct Urca is small compared to the contribution of the nucleon direct Urca in the non superfluid case, the hyperon direct Urca might become important if the nucleons form superfluid pairs. If however the hyperons become also superfluid, then their contribution is again negligible. The superfluid phase transition of hyperons has unfortunately not been studied so far since it is rather difficult to implement superfluidity in relativistic treatments with hyperons. We therefore neglect this contribution to the neutrino emissivity.

The pion condensation was suggested by Migdal (1971), Scalapino (1972), and Sawyer (1972) and then considered by many authors (e.g. Brown & Weise 1976, Migdal 1978, and Migdal et al. 1990). In the last years, some arguments against the occurrence of pion condensation in neutron stars were given in the literature (see, for instance, Brown et al. 1995). These arguments are generally based on the rather strong increase of the Landau-Migdal parameter g' with the nucleon density. However other effects which might be important for the pion condensation problem (cf. Migdal et al. 1990) were not incorporated. Thus one may conclude that the question whether a pion condensate occurs in neutron stars is still not settled (see Ericson & Weise 1988 and Kunihiro et al. 1993 for extensive reviews).

We shall therefore use models both with and without pion condensates applying two parametrizations of $\tilde{\omega}^2(n)$ (see Sect. 2.1).

Additionally the neutrino emissivity in kaon condensation, which is now favored by various authors (e.g. Brown et al. 1988 and Thorsson et al. 1995) as well as the critical density for the onset of condensation are quite similar to the case of pion condensation. The additional $\tan(\Theta_c)$ -factor in the kaon condensation case, where $\Theta_c \simeq 0.223$ is the Cabibbo-angle, is partly compensated by a probably larger value of the suppression-factor Γ^4 due to a possible suppression of the correlations between strange and non-strange baryons. The cooling curves for the models with kaon condensation look quite similar (see, for example, Umeda et al. 1994 and Schaab et al. 1996a). We shall therefore study only pion condensation.

Above threshold density for pion condensation n_c^π , the contribution of eq. (1) to the neutrino emissivity of the MU process is to be supplemented by the corresponding pion Urca processes (cf. Maxwell et al. 1977, VS84). For the latter processes we use a simplified expression including the nucleon–nucleon correlation effect in the πNN vertices (VS84, Migdal et al. 1990),

$$\begin{aligned} \epsilon_\nu^{(PU)} &\simeq 1.5 \times 10^{27} \frac{p_{Fn}(n)}{m_\pi} \left(\frac{m_N^*}{m_N} \right)^2 \Gamma^4 T_9^6 \sin^2 \theta \\ &\times \frac{\text{erg}}{\text{cm}^3 \text{ sec}}, \end{aligned} \quad (9)$$

for densities $n > n_c^\pi$. Here the neutron Fermi momentum is expressed in units of m_π , and $\sin \theta \simeq \sqrt{2|\tilde{\omega}^2|/m_\pi^2}$ for $\theta \ll 1$, whereas at large densities ($n \gg n_c^\pi$) a well-developed condensate implies $\theta \rightarrow \pi/2$. We shall use an ansatz that interpolates between these two extremes. Since $\pi^{+,-}$ condensation probably reduces the energy gaps of the superfluid states by an order of magnitude (see Takatsuka & Tamagaki 1980), we assume, for the sake of simplicity, that superfluidity vanishes above n_c . Finally we note that though the PU processes have genuinely one–nucleon phase–space volumes, their contribution to the resulting emissivity is suppressed relative to the direct Urca by an additional Γ^2 vertex factor due to existence of the additional πNN vertex in the former case.

The modifications of energy density and pressure due to the pion condensation are taken into account as

$$\rho_\pi \simeq -\frac{|\tilde{\omega}^2(n)| \sin^2(\theta)}{2} \times m_\pi^2, \quad P_\pi = n^2 \frac{\partial}{\partial n} \left(\frac{\rho_\pi}{n} \right), \quad (10)$$

where, again, $\tilde{\omega}^2$ is given in the units m_π^2 .

3. Stellar Composition and Structure

The general relativistic equations of stellar structure and thermal evolution (cf. Thorne 1977) were solved via a numerical code based on an implicit finite difference scheme handled by a Newton-Raphson algorithm. Details can be found in Schaab et al. (1996a). The physical input quantities, are summarized in Table 2. Besides the new neutrino–emission processes discussed in this paper, we include in the simulations the traditional neutrino processes too, which are discussed in greater detail by Schaab et al. (1996a).⁵

Table 2. Input quantities used for the cooling simulations

Parameter	References
Equations of state:	
crust	Baym et al. (1971), Negele & Vautherin (1973)
core	see Table 3
Superfluidity	see Table 4
Heat capacity	Van Riper (1991), Shapiro & Teukolsky (1983)
Thermal conductivities:	
crust	Itoh et al. (1984), Itoh (1983), Mitake et al. (1984)
core	Gnedin & Yakovlev (1995)
Neutrino emissivities:	
pair-, photon-, plasma-processes	Itoh et al. (1989)
bremsstrahlung in the crust	Itoh & Kohyama (1983), Pethick & Thorsson (1994)
bremsstrahlung in the core	FM79, Maxwell (1979)
MU-FM79	FM79
or instead: MU-VS86	eq. (1), VS86
NPBF and PPBF processes	eq. (4,5), Voskresensky & Senatorov (1987)
DU-process	eq. (8), Lattimer et al. 1991
PU-process	eq. (9), VS84
photosphere	Van Riper (1988)

⁵ The two-nucleon neutral current processes (bremsstrahlung-processes) are also modified by in-medium effects (VS86). Their contribution is however much smaller than the corresponding contribution of the MU-VS86 process. These modifications are therefore not implemented here.

3.1. Equation of State

For the outer and inner crust we adopt the equations of state of Baym et al. (1971) and Negele & Vautherin (1973). The transition density between the ionic crust and the core of a neutron star is assumed to be $\rho_{\text{tr}} = 1.7 \times 10^{14} \text{ g cm}^{-3}$ (Pethick et al. 1995). The high density matter in the cores of neutron stars is described by a collection of modern equations of state, which consists of a non-relativistic Schrödinger-based model as well as three relativistic field theoretical ones. The details of these models are summarized in Table 3. One of the significant differences between these equations of state is that the non-relativistic model treats neutron star matter as being composed of neutrons and protons only (which are in β -equilibrium with leptons). The relativistic models account for all hyperon states that become populated in the cores of neutron stars as predicted by theory (Glendenning 1985). Dynamical two-nucleon correlations calculated from the relativistic scattering T-matrix in matter are contained in the relativistic Brueckner-Hartree-Fock (RBHF) equation of state. The underlying one-boson-exchange interaction is Brockmann’s potential “B”. At densities larger than about three times normal nuclear matter density it has been joined with a relativistic Hartree-Fock (RHF) equation of state (Huber et al. 1994, 1996). The non-relativistic treatment of the EOS leads generally to a softer EOS than the relativistic treatment. However, since in the non-relativistic case one takes only nucleons and leptons into account the relativistic EOS’s with hyperons become almost as soft as the non-relativistic EOS’s. Both treatments therefore mainly differ in the resulting composition. This can be important for the nucleon and hyperon direct Urca (see Sect. 2.3). The equations of state are shown in Fig. 4 and the corresponding neutron star sequences in Fig. 5.

Table

3. Collection of nuclear equations of state (EOSs). Abbreviations: nvar=nonrelativistic variational, RH=relativistic Hartree, RHF=relativistic Hartree-Fock, RBHF=relativistic Brueckner-Hartree-Fock.

EOS	Composition	Interaction	Method	Ref.
UV ₁₄ +UVII	p,n,e, μ	Urbana V ₁₄ +VII	nvar	Wiringa et al. (1988)
HV	p,n, Λ , Σ , Ξ ,e, μ	σ, ω, ρ	RH	Weber & Weigel (1989)
RBHF(B)+HFV	p,n, Λ , Σ , Ξ , Δ ,e, μ	$\sigma, \omega, \pi, \rho, \eta, \delta$	RBHF, RHF	Huber et al. (1994)
G ₃₀₀	p,n, Λ , Σ , Ξ ,e, μ	σ, ω, ρ	RH	Glendenning (1989)

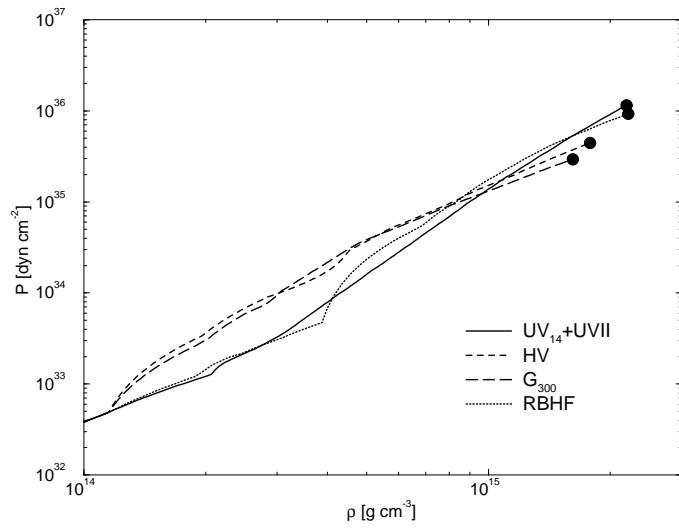


Fig. 4. Equations of state (pressure versus energy density) used in this paper. The dots refer to the maximal central densities reached in the most massive neutron stars constructed for these EOS's. The modifications caused by a pion condensate alter the EOS's only insignificantly on this scale and are thus not shown.

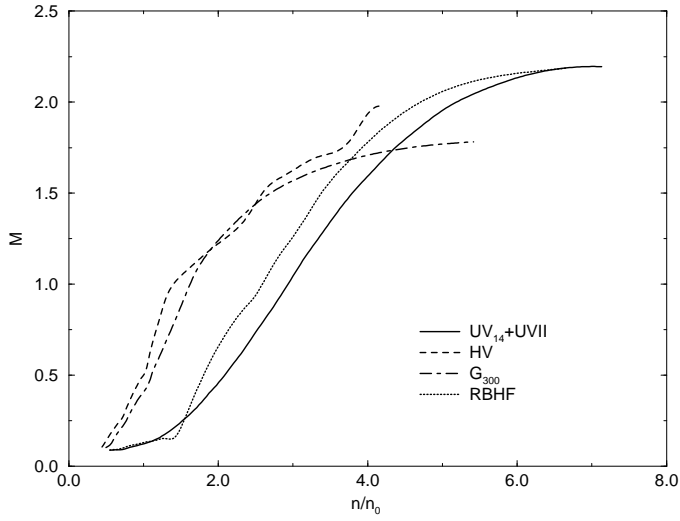


Fig. 5. Star masses in units of solar mass versus central star density for the EOS's used in this paper.

3.2. Superfluidity

The following superfluid regions inside neutron stars are taken into account:

- $7 \times 10^{11} \text{ g cm}^{-3} \leq \rho \leq 2 \times 10^{14} \text{ g cm}^{-3}$: neutrons in 1S_0 -pair state,
- $2 \times 10^{14} \text{ g cm}^{-3} \leq \rho \leq 4 \times 10^{14} \text{ g cm}^{-3}$: protons in 1S_0 -pair state, and
- $2 \times 10^{14} \text{ g cm}^{-3} \leq \rho \leq 5 \times 10^{15} \text{ g cm}^{-3}$: neutrons in 3P_2 -pair state.

The proton gap is taken from Wambach et al. (1991), those of 1S_0 - and 3P_2 -paired superfluid neutrons are from Ainsworth et al. (1989) and Amundsen & Østgaard (1985), respectively. Details are given in table 4. It should be emphasized that the extension of the superfluid density regime depends on the equation of state. The above values are computed for the HV equation of state, and Fig. 6 displays the profiles of the superfluid gaps for this particular model.

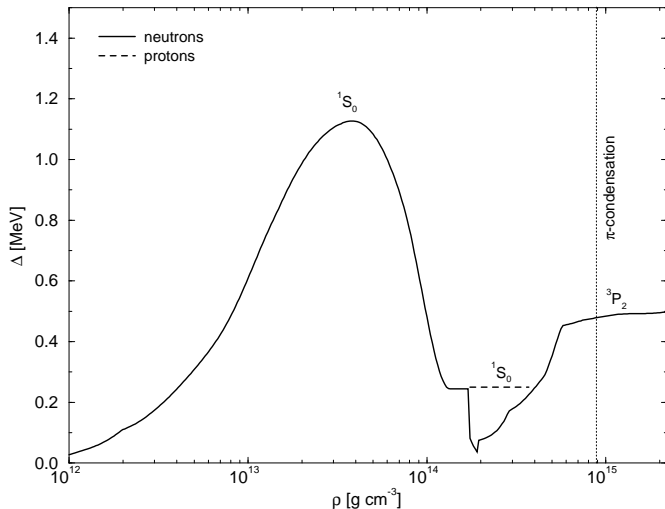


Fig. 6. Superfluid energy gaps computed for the HV EOS. We neglect superfluidity in the models where pion condensation is allowed for densities $n > n_c^\pi = 3n_0$ (dotted line).

Table 4. Maximal gap energies, $\Delta_{\text{sf}}^{\text{max}}$, critical temperatures, T_c^{max} , and density ranges, ρ , in neutron star matter computed for the HV equation of state

	Neutron 1S_0	Neutron 3P_2	Proton 1S_0
$\Delta_{\text{sf}}^{\text{max}}$ [MeV]	1.13	0.62	0.25
T_c^{max} [10^9 K]	7.4	0.8	1.6
ρ [g cm^{-3}]	$7 \times 10^{11} - 2 \times 10^{14}$	$2 \times 10^{14} - 5 \times 10^{15}$	$2 \times 10^{14} - 4 \times 10^{14}$
Reference	Ainsworth et al. (1989)	Amundsen & Østgaard (1985)	Wambach et al. (1991)

Because the pairing gaps are not too accurately known, we shall also study cooling scenarios of superfluid neutron stars where the magnitudes of the gaps are varied in an *ad hoc* fashion about their theoretically determined values. This procedure may serve to reveal the dependence of our theoretical cooling scenarios on the uncertainties associated with the superfluid gaps.

As already mentioned in Sect. 2.1, the superfluid gaps are reduced by an order of magnitude in $\pi^{+,-}$ condensed matter (see Takatsuka & Tamagaki 1980). We therefore neglect superfluidity in pion condensed matter completely. In passing we emphasize that in a more elaborate treatment, one needs to pay attention to the effects of interactions between $\pi^{+,-}$ and π^0 condensates, simultaneous appearance of K^- and \bar{K}^0 condensates (Brown et al. 1994, Kolomeitsev et al. 1995) which affect the neutron and proton gaps differently. Furthermore, neutron–proton pairing in the 3D_2 -triplet state for almost symmetric nuclear matter⁶ may dominate the traditionally considered 3P_2 pairing (Alm et al. 1996).

Finally when performing numerical cooling calculations for superfluid neutron stars, we follow the traditional procedure by suppressing the two–nucleon reaction neutrino emissivities, the thermal conductivity, and the heat capacity of the nucleonic constituents of the stellar matter by factors which behave like $\exp(-\Delta_{n(p)}/k_B T)$ for $T \ll T_c$, where $\Delta_{n(p)}$ denotes the gap, T the temperature (see Maxwell 1979, Gnedin & Yakovlev 1995)⁷.

4. Results and Discussion

4.1. Observational Data

Compact X-ray sources have been detected by the X-ray observatories Einstein, EXOSAT and ROSAT during the last two decades. Among them, 14 X-ray sources – observed at least by one of these satellites – were identified as radio–pulsars (with the exception of Geminga, which is known to be radio–quiet). The information obtained from these detections is not always sufficient to extract the effective surface temperature of the corresponding pulsar. Therefore this sample of pulsars is divided into three different categories (see Ögelman 1995):

1. The detection of three pulsars (PSR’s 1706-44, 1823-13, and 2334+61) contain too few photons for spectral fits. The specified luminosities are calculated by using the totally detected photon flux. These pulsars are marked with triangles in the figures that will be discussed below.

⁶ In neutron star matter with hyperons based on relativistic EOS’s the neutron and proton fractions tend to each other with increasing density and are almost equal in the high density limit (cf. Weber & Weigel 1989 and Glendenning 1989). One must distinguish this case from the nonrelativistic treatment without hyperons, where in the presence of kaon condensation isospin symmetric matter is preferred (cf. Thorsson et al. 1994).

⁷ For the 3P_2 state this is rigorously true only for isotropic system (see Anderson & Morel 1961, Muzikar 1980, and Page 1995).

2. The spectra of seven pulsars, including the Crab pulsar (PSR 0531+21), can only be fitted by a power-law-type spectrum, or by a blackbody spectrum with very high effective temperature and effective areas much smaller than the neutron star surface. Their X-ray emission is predominated by magnetospheric emission. Therefore, the temperatures, determined from the spectral fits, are probably too high. Pulsars of this type are marked with dots.
3. Finally, there are four pulsars, i.e., 0833-45 (Vela), 0656+14, 0630+18 (Geminga), and 1055-52, allowing two-component spectral fits. The softer blackbody component is believed to correspond to the actual surface emission of the neutron star, while the harder blackbody (or power-law) component may be due to magnetospheric emission. These pulsars are marked with squares.

An overview of the observed luminosities and pulsar ages is contained in Table 5.

Table 5. Luminosities, L , and spin-down ages, τ , of pulsars

Pulsar	Name	$\log \tau$ [yr]	$\log L$ [erg/s]	Reference
not enough data available for spectral analysis				
1706-44		4.25	32.8 ± 0.7	Becker et al. (1992)
1823-13		4.50	33.2 ± 0.6	Finley & Ögelman (1993)
2334+61		4.61	33.1 ± 0.4	Becker (1993)
power-law-type spectra or spectra with only a high temperature component				
0531+21	Crab	3.09	33.9 ± 0.2	Becker & Aschenbach (1995)
1509-58	SNR MSH 15-52	3.19	33.6 ± 0.4	Seward et al. (1983), Trussoni et al. (1990)
0540-69		3.22	36.2 ± 0.2	Finley et al. (1993)
1951+32	SNR CTB 80	5.02	33.8 ± 0.5	Safi-Harb & Ögelman (1995)
1929+10		6.49	28.9 ± 0.5	Yancopoulos et al. (1993), Ögelman (1995)
0950+08		7.24	29.6 ± 1.0	Seward & Wang (1988)
J0437-47		8.88	30.6 ± 0.4	Becker & Trümper (1993)
spectrum dominated by a soft component				
0833-45	Vela	4.05	32.9 ± 0.2	Ögelman et al. (1993)
0656+14		5.04	32.6 ± 0.3	Finley et al. (1992)
0630+18	Geminga	5.51	31.8 ± 0.4	Halpern & Ruderman (1993)
1055-52		5.73	33.0 ± 0.6	Ögelman & Finley (1993)

4.2. Impact of Softening of Pion Exchange Modes and Intermediate Pion Decay on Cooling

In Figs. 7–9 we show the impact of the medium effects on the cooling of neutron stars of different masses. Fig. 7 compares the mass dependence of the neutrino cooling rates L_ν/C_V associated with MU-FM79 and MU-VS86 for non-superfluid matter. For the solid curves, the neutrino emissivity in pion-condensed matter (threshold density $n_c^\pi = 3n_0$) is taken into account according to eq. (9) and (1) with the parameter $\alpha = \sqrt{2}$. The dashed curves correspond to the case where no pion condensation is allowed. As one sees the medium polarization effects included in MU-VS86 may result in three order of magnitude increase of the cooling rate for the most massive stars. Even for stars of a low mass the cooling rate of MU-VS86 is still few times larger than for MU-FM79 because even in this case the more efficient rate is given by the reactions shown by the right diagram in Fig.1. The cooling rates of the $1.8M_\odot$ mass models with and without pion condensate differ only by a factor of 5.

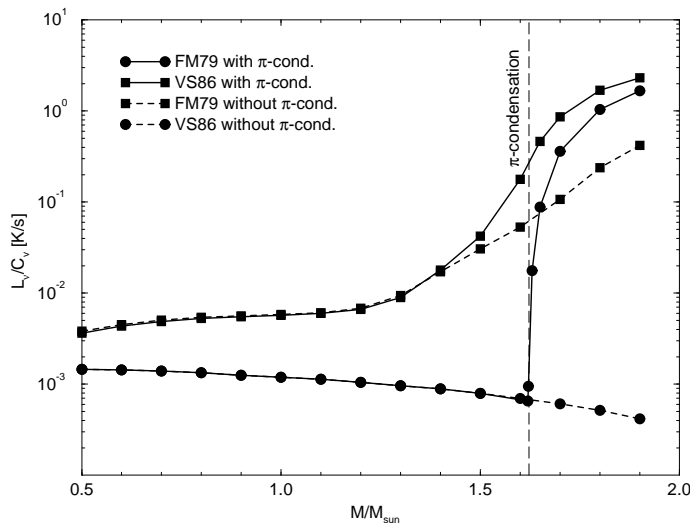


Fig. 7. Cooling rate due to neutrino emission as a function of star mass for a representative temperature of $T = 3 \times 10^8$ K. The solid curves refer to cooling via MU-FM78+PU and MU-VS86+PU in pion-condensed (threshold density $n_c = 3n_0$) matter. The dashed curves refer to cooling without pion condensation. Superfluidity is neglected here.

One sees that the cooling rates for the FM79 result vary significantly (by about three orders of magnitude!) only over a rather small mass range from the models without pion condensation to the ones with pion condensation. The cooling rates are rather independent of star mass below the critical mass value (i.e., $M = 1.63 M_\odot$) at which the transition into the pion-condensed phase occurs, and show a flattening

behavior above. The resulting cooling behavior of neutron stars of several selected masses is shown in the left graph of Fig. 8. These curves are quite similar for models without pion condensation. Stars which are sufficiently heavy such that a pion condensate can develop in their cores evolve along cooling tracks that are rather different from the former, provided the stars are older than about 10 years. We illustrate this for two representative star masses, $M = 1.7$ and $M = 1.9 M_{\odot}$. Depending on star mass, the resulting photon luminosities are basically either too high or too low to account for the bulk of observed pulsar luminosities, which tends to be a general feature of cooling calculations no matter what kind of enhanced cooling mechanism are being studied (cf. Schaab et al. 1996a).

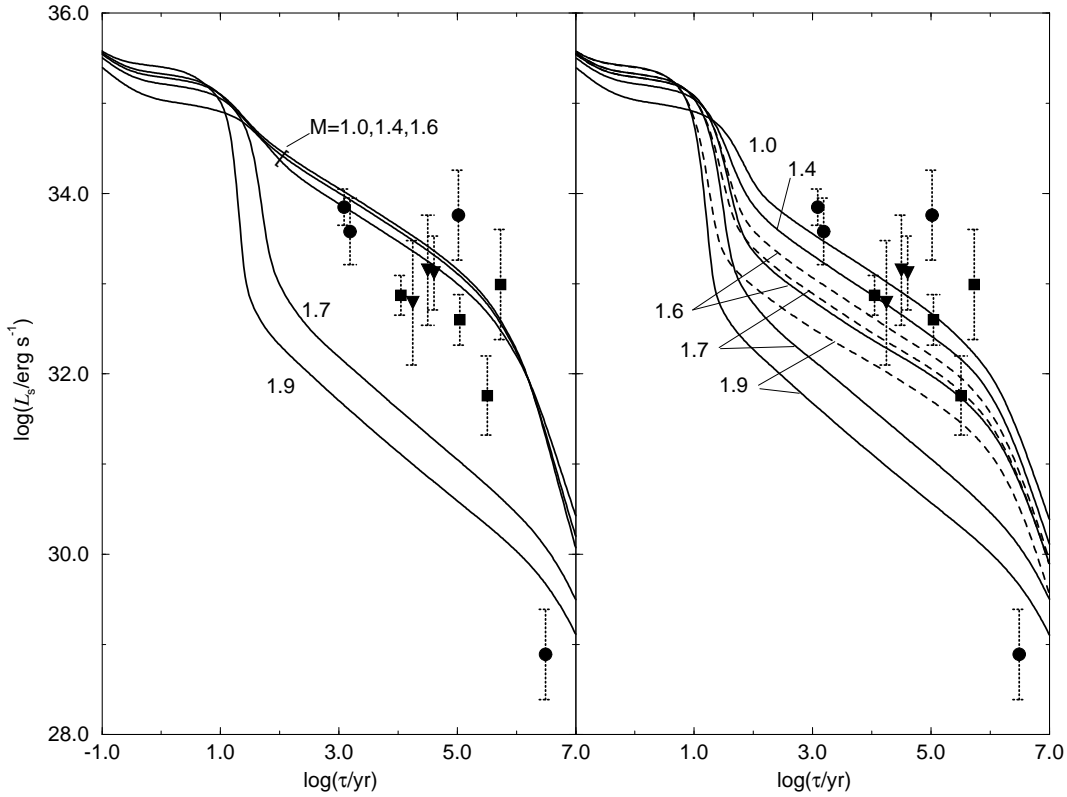


Fig. 8. Cooling of non-superfluid neutron star models of different masses constructed for the HV EOS. The two graphs refer to cooling via MU-FM79+PU (left) and MU-VS86+PU (right). In both cases, pion condensation is taken into account for the solid curves where $n > n_c^\pi = 3n_0$. The dashed curves in the right graph refer to the $\tilde{\omega}^2$ parametrization without pion condensation. The observed luminosities are labeled in Fig. 14.

The situation changes if the modified Urca process with the medium modifications of the pion-exchange interaction, appropriate vertex corrections, and the

radiation from the intermediate states (MU-VS86) is included. Now the cooling rates vary smoothly with star mass (see Fig. 7) such that the gap between standard and enhanced cooling is washed out. More quantitatively, by means of varying the star mass between 1.0 and 1.6 M_{\odot} , one achieves agreement with a large number of observed data points, see right graph of Fig. 8. This is true for both choices of the $\tilde{\omega}^2$ parametrization, independently whether a pion condensation can occur or not. The two parametrizations differ only in the range which is covered by the cooling curves. The only pulsars which do not agree with the cooling curves are the hot PSR's 1055-52 and 1951+32 and the rather cold object PSR 1929+10. The high luminosities of the former two may be due to internal heating processes, which leads to delayed cooling for star ages $t > 10^5$ yr (see for example Shibazaki & Lamb 1989, Sedrakian & Sedrakian 1993, Reisenegger 1995, Van Riper et al. 1995, Schaab et al.). To achieve agreement with the extremely low-luminosity object PSR 1929+10, the inclusion of strong magnetic fields in the atmosphere (see Van Riper 1991) or other fast cooling processes, like direct Urca etc. seems necessary (cf. Fig. 11 and Schaab et al. 1996a).

Next we shall study the modified Urca process in superfluid matter. Results are displayed in Fig. 9. The processes NPBF and PPBF, which will be discussed later, have been artificially forbidden. The value of the neutron 3P_2 gap from Amundsen & Østgaard (1985) is rather large such that the difference between slow (MU-FM79, left graph) and intermediate (MU-VS86, right graph) cooling is almost indistinguishable. Superfluidity strongly suppresses the neutrino emission rates from stars containing a superfluid core, which thus delays cooling. As it was the case for standard cooling, the thermal evolution of superfluid stars is rather insensitive against variations of the star's mass. However, as soon as charged pions condense in the core of a neutron star, superfluidity disappears and the much higher neutrino emission rates cause the cooling curves to drop down by more than two orders of magnitude. For the model which allows for pion condensation, this occurs when the star's mass is varied from 1.6 to 1.7 M_{\odot} . In principle, it appears possible to achieve agreement between the body of observed cooling data and the cooling simulations by properly varying the star's mass in an extremely narrow range. Surely, such a procedure is not very satisfying because it requires an extreme fine-tuning of the mass of a star. As we shall see below, the superfluid state allows for other neutrino-emitting processes which decisively influence the cooling of stars and thus provide other, less stringent conditions by means of which agreement with the observed data can be achieved.

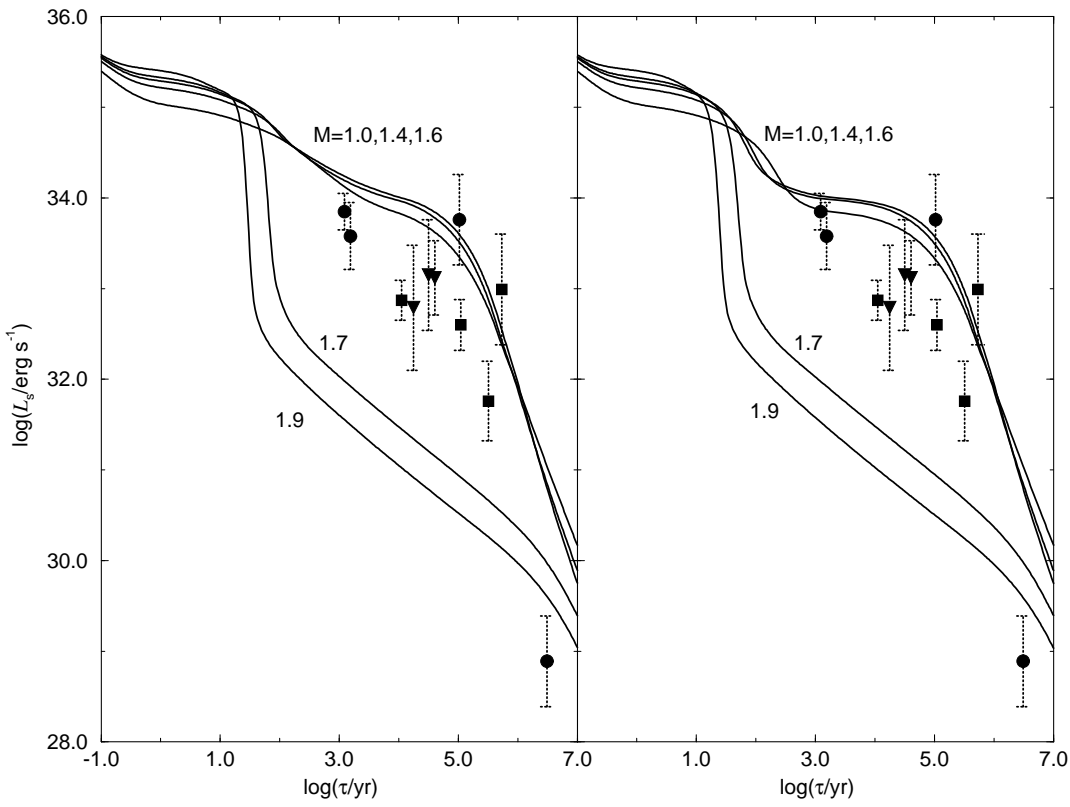


Fig. 9. Same as Fig. 8 but for superfluid neutron star models. NPBF and PPBF are not incorporated. The observed data are labeled in Fig. 14.

4.3. Superfluid Pair Breaking and Formation

To demonstrate the relevance of the superfluid pair breaking and formation processes for the cooling of neutron stars, in the first step, we implement these two processes into standard cooling calculations. In these calculations the FM79 result for the modified Urca process is used. No further processes, like DU or PU is taken into account here. The results are shown in Fig. 10. One sees that NPBF and PPBF reduce the photon luminosity of neutron stars significantly for star ages between about $1 < t < 10^6$ yr. The acceleration of the cooling is mostly due to the superfluid transition of the neutrons in the crust since the gap energy for this transition is 1.13 MeV compared to 0.25 MeV for the protons in the core (see Tab. 4) and the value of Δ/T at $T = T_c$ is 0.57 compared to 0.12 for the neutrons in the core (see Sec. 2.2). One can also see that the importance of the NPBF process increases with decreasing gap energy of the 1S_0 -neutron-pairing. For $t > 10^6$ yr the influence of NPBF and PPBF becomes rather weak and cooling via photon emission from the star's surface becomes the dominant process. As a result, the solid and dashed curves in Fig. 10 are almost identical for $t > 10^6$ yr.

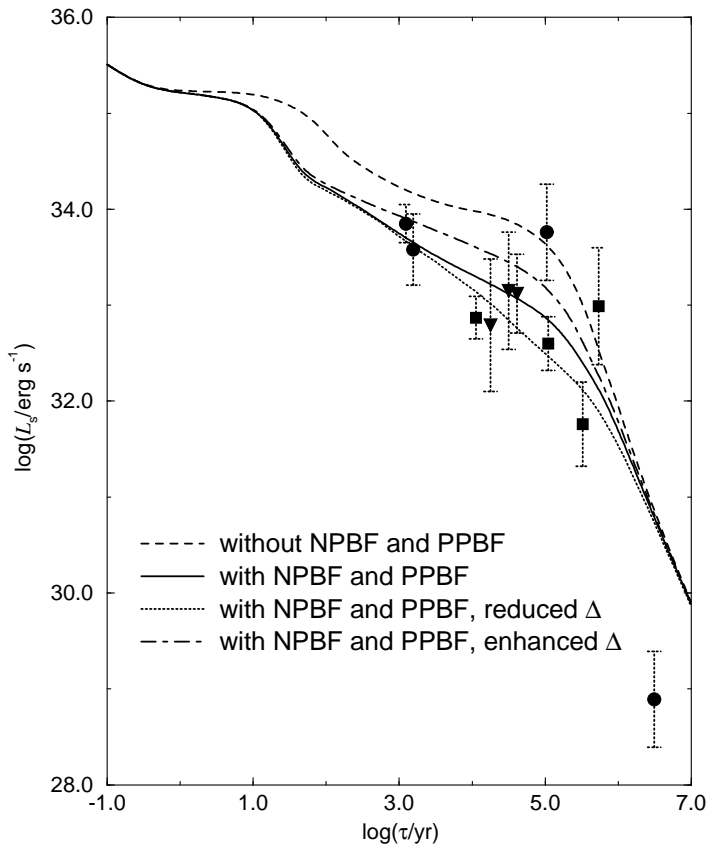


Fig. 10. Cooling of neutron stars of mass $M = 1.4M_{\odot}$ constructed for the HV EOS. The curves correspond to standard cooling (MU-VS86 and PU ignored) with (solid curve) and without (dashed curve) NPBF+PPBF. The gap energy of the 1S_0 -neutron-pairing is arbitrarily enhanced (dotted curve) or reduced (dashed-dotted curve), respectively by a factor of 2 in order to demonstrate the dependency of the rates on the gap energy. The observed data are labeled in Fig. 14.

4.4. Final Results and Influence of Equation of State

We turn now to cooling simulations where the MU, NPBF, PPBF, DU and PU take place simultaneously. Fig. 11 shows the cooling tracks of stars of different masses, computed for the HV equation of state. The DU process is taken into account in the right graph, whereas it is neglected in the left graph. The solid curves refer again to the $\tilde{\omega}^2$ -parameterization with phase transition to a pion condensate, the dashed curves to the one without phase transition. For masses in the range between 1.0 and 1.6 M_{\odot} , the cooling curves pass through most of the data points. We again recognize a photon luminosity drop by more than two orders of magnitude of the 1.7 M_{\odot} mass star with pion condensate, due to vanishing of the superfluidity as

a consequence of pion condensation. This drop is even larger if the DU is taken into account (right graph, this allows to account for the photon luminosity of PSR 1929+10).

A comparison with the observed luminosities shows that one gets quite good agreement between theory and observation if one assumes that the masses of some of the underlying pulsars are different from the canonical value, $M = 1.4 M_{\odot}$. Since the masses of these pulsars are not known, no further conclusions about the actually operating cooling mechanism of these pulsars can be drawn yet. Future mass determinations of these objects will change the situation. The only two stars whose photon luminosities cannot be accounted for by the new processes studied here are the rather hot pulsars PSR 1055-52 and PSR 1951+32. Again, as mentioned above, their temperatures may be explained by internal heating.

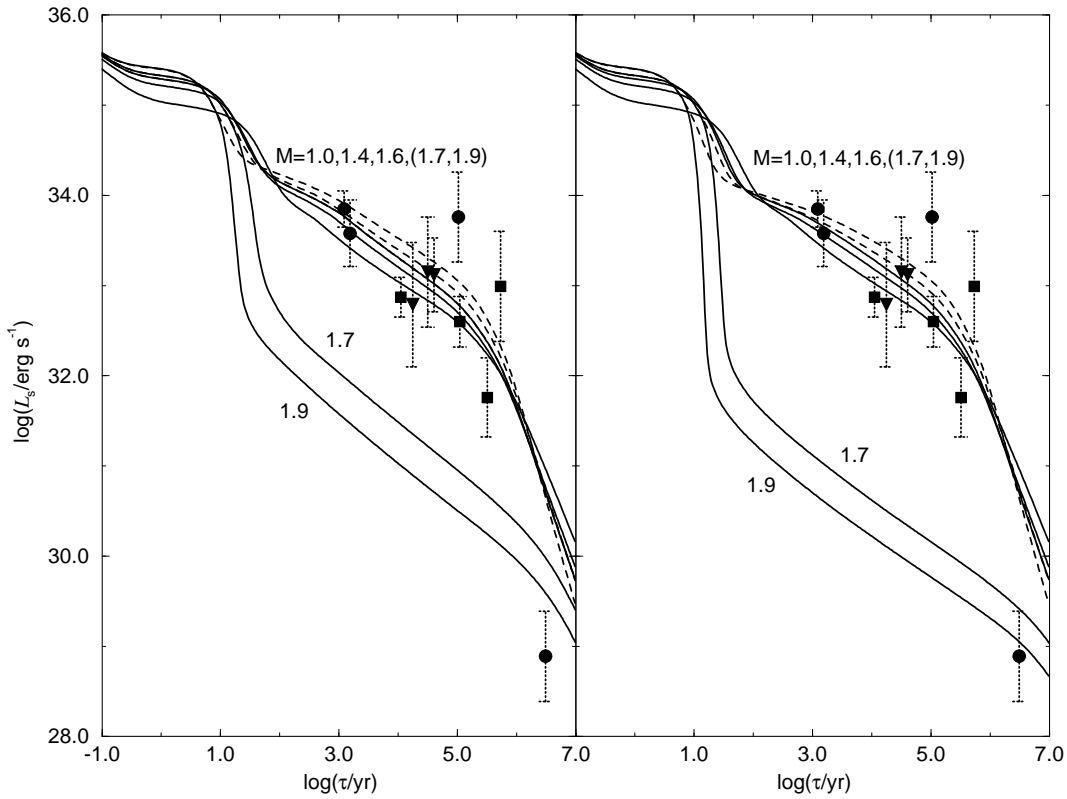


Fig. 11. Cooling of neutron stars with different masses constructed for the HV EOS. The cooling processes are MU-VS86, PU (only solid curves), NPBF, PPBF, and DU (only in the right graph). The dashed curves refer to the $M = 1.7$ and $1.9 M_{\odot}$ models without pion condensate. The observed data are labeled in Fig. 14.

To explore the impact of somewhat smaller superfluidity gaps on cooling, we arbitrarily reduced the gap by a factor of 6. Its major effect is a drop in the cooling curves of the 1.0 to 1.6 M_{\odot} mass stars and of the 1.7 and 1.9 M_{\odot} mass stars without pion condensate (dashed curves). This would lead to better agreement with the low-temperature pulsar 0630+18 (Geminga) (see Fig. 12).

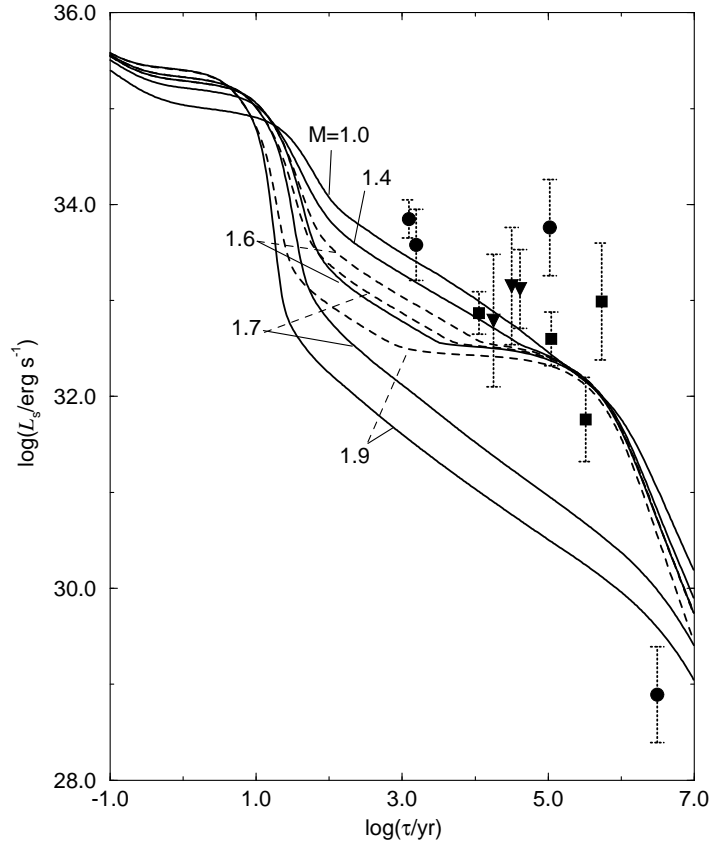


Fig. 12. Same as left graph of Fig. 11 but with the original ${}^3\text{P}_2$ gap by Amundsen & Østgaard (1985) reduced by a factor of 6. The observed data are labeled in Fig. 14.

So far we have selected a particular model for the equation of state of neutron star matter, i.e. HV, and studied the dependence of the cooling curves on the star's mass. The influence of different models for the equation of state on cooling is shown in Figs. 13–15. Fig. 13 displays the cooling behavior computed for a representative non-relativistic model for the equation of state, $\text{UV}_{14} + \text{UVII}$. The general qualitative features obtained for HV carry over to this case, except that the temperature drop occurs now at a lower mass threshold. For that reason the 1.1 M_{\odot} mass star is already anomalously cold. Because of the relatively high neutron fraction of the

UV₁₄+UVII compared to relativistic EOS's the superfluid phase does not reach to the center of the 2.1M_⊙ mass star in this particular model of Amundsen & Østgaard (1985). This causes the luminosity drop to occur also for the model without pion condensate (dashed curve). The high neutron fraction, or identically the low proton fraction, has also the effect that the DU process cannot occur.

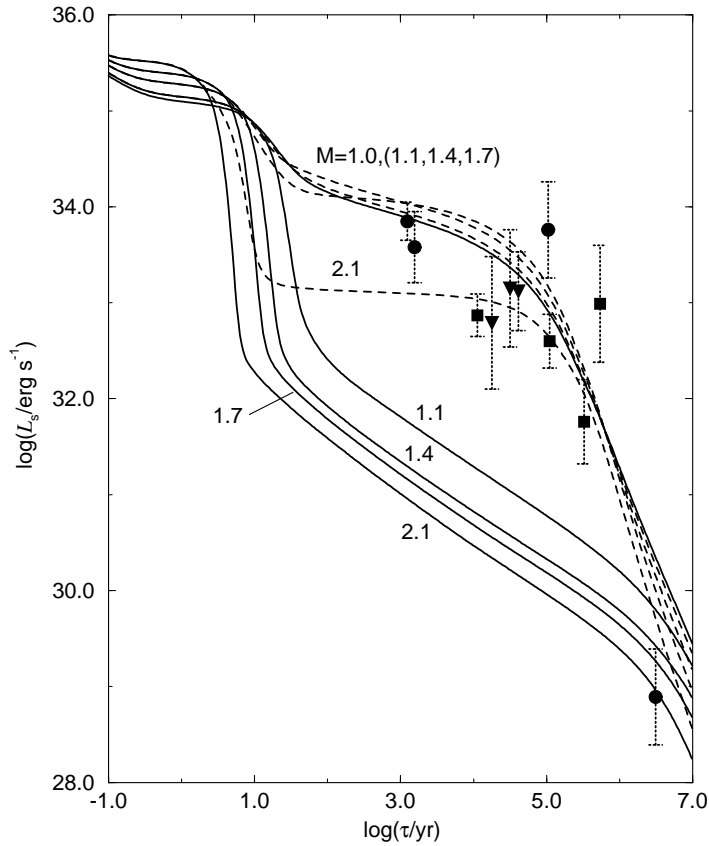


Fig. 13. Cooling of neutron stars of different masses constructed for the UV₁₄+UVII EOS. The cooling processes are MU-VS86, PU (only solid curves), NPNF, and PPBF. The observed data are labeled in Fig. 14.

The cooling curves constructed for RBHF, shown in Fig. 14, are rather similar to those of UV₁₄+UVII though the underlying microscopic theories employed to determine these two models for the equation of state are completely different. We recall that the former, RBHF, is based on a parameter-free relativistic Brueckner-Hartree-Fock calculation while the latter, UV₁₄+UVII, was derived in the framework of a non-relativistic many-body variational calculation. In both cases, however, dynamical nucleon-nucleon correlations are taken into account, which – as a general feature – tend to soften the equation of state at intermediate nuclear densities, both in the

relativistic as well as in the non-relativistic case (Fig. 4). For that reason both of these models for the equation of state lead to similar slopes of star mass as a function of central star density (see Fig. 5) and similar cooling behaviors. With respect to the differences between RBHF and $UV_{14}+UV_{VII}$, the former is harder than the latter. Therefore the magnitude of the temperature drop for increasing star masses is smaller. For both of these models, pion condensation set in at rather low neutron star masses, causing already the rather light neutron stars ($M \sim 1.1 M_{\odot}$) to cool very rapidly. In contrast to the $UV_{14}+UV_{VII}$ EOS, the RBHF has large proton fractions at high densities causing the superfluid phase to reach to the center of the star for all masses and allowing for the DU process. The cooling tracks for the $\tilde{\omega}^2$ -parameterization without pion condensation and the ones with the DU process are similar to the cooling tracks for the HV EOS. Thus, we can restrict ourselves to the pion condensation case without DU process.

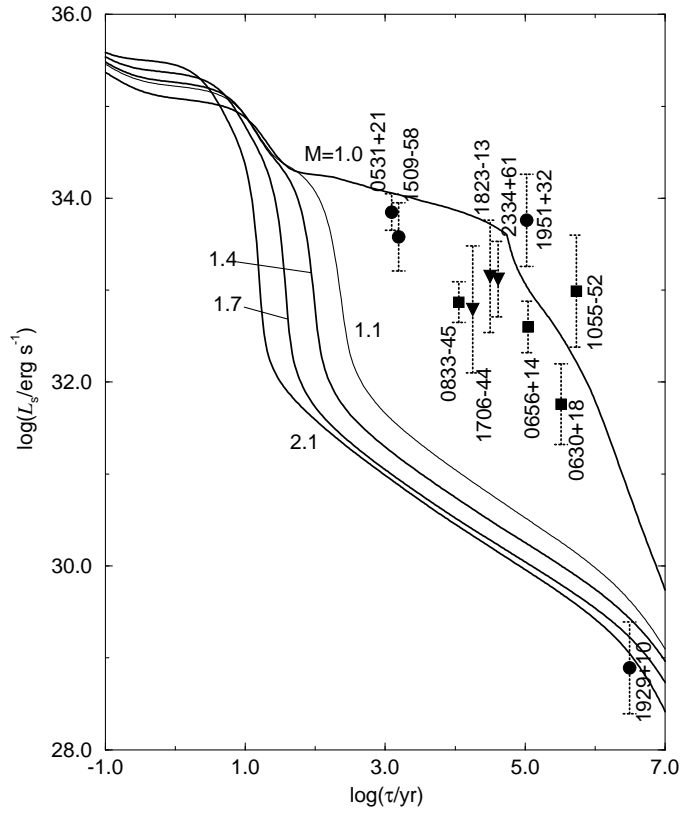


Fig. 14. Cooling of neutron stars of different masses constructed for the RBHF EOS. The cooling processes are MU-VS86, PU, NPBF, and PPBF. The observed data are labeled in Fig. 14.

Besides HV, we employ a second model, labeled G_{300} , for the equation of state derived in the framework of relativistic mean-field theory. Both equations of state are rather similar, as can be seen in Figs. 4 and 5, and so are the corresponding cooling curves, Fig. 15. Again only the pion condensation case without DU process is studied.

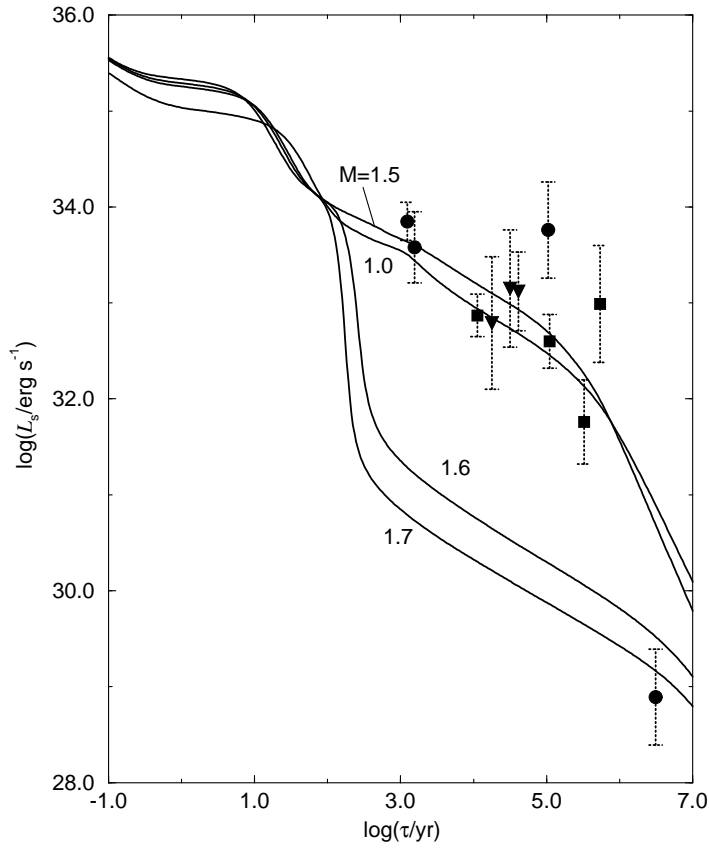


Fig. 15. Same as Fig. 14 but for the G^{300} EOS. The observed data are labeled in Fig. 14.

5. Summary

Two recalculated neutrino-emitting processes in dense neutron star matter, i.e., the modified Urca process and the superfluid pair breaking and formation processes, have been implemented in numerical cooling simulations of neutron stars. Our major finding is that standard cooling processes supplemented with the medium effects enables one to achieve theoretical agreement with a large fraction of the observed pulsar luminosities, which — subject to uncertainties in the equation of state and

transport properties of superdense matter — seems to be a problem for the standard cooling scenario alone (cf. Schaab et al. 1996a). In particular it is possible to account for the low temperatures of PSRs 0833-45 (Vela), 0656+14, and 0630+18 (Geminga). Secondly, the new processes studied here provide a crossover between standard cooling and the so-called fast cooling scenarios of neutron stars and thus can be viewed as “*intermediate*” cooling scenarios.

Acknowledgements. We would like to thank K. A. Van Riper for sending us his table of the temperature gradient in the photosphere as a function of the surface temperature, which was used in our cooling calculations. We are also grateful to the referee for his valuable comments. Furthermore, we thank B. Friman and D. Page for helpful discussions. D.V. thanks the GSI and Rostock University for their hospitality and financial support and acknowledges financial support from the International Science Foundation (grant N3W000).

References

- Ainsworth, T., Wambach, J., Pines, D., 1989, Phys. Lett., **B 222**, 173.
- Alm, T., Röpke, G., Sedrakian, A. D., Weber F. 1996, Nucl. Phys., **A604**, 491.
- Amundsen, L., Østgaard, E., 1985, Nucl. Phys., **A442**, 163.
- Anderson, P., Morel, P., 1961, Phys. Rev., **123**, 1911.
- Bahcall, J.N., Wolf, R.A., 1965, Phys.Rev. **B140**, 1445.
- Baym, G., Pethick, C., Sutherland, P., 1971, ApJ, **170**, 299.
- Becker, W., 1993, IAU Circ., **No. 5805**.
- Becker, W., Aschenbach, B., 1995, in *The Lives of the Neutron Stars*, edited by M. Alpar, Ü. Kiziloglu, J. van Paradijs, Kluwer, Dordrecht, p.47.
- Becker, W., Trümper, J., 1993, Nature, **365**, 528.
- Becker, W., Predehl, P., Trümper, J., Ögelman, H., 1992, IAU Circular, **No. 5554**.
- Blaschke, D., Röpke, G., Schulz, H., Sedrakian, A., Voskresensky, D., 1995, MNRAS, **273**, 596.
- Boguta, J., 1981, Phys. Lett., **106B**, 255.
- Brown, G. E., Weise, W., 1976, Phys. Rep., **27**, 1.
- Brown, G. E., Kubodera, K., Page, D., Pizzochero, P., 1988, Phys. Rev., **D37**, 2042.
- Brown, G. E., Lee C. H., Rho, M., Thorsson, V., 1994, Nucl. Phys., **A567**, 937.
- Brown, G. E., Buballa, M., Li, Z. B., Wambach, J., 1995, Nucl. Phys., **A593**, 295.
- Chen, J. M. C., Clark, J. W., Davé, R. D., Khodel, V. V., 1993, Nucl. Phys., **A555**, 59.
- Dyugaev, A. M., 1975, Pisma v ZhETF, **22**, 181, in Engl.: 1975, JETP Lett., **22**, 83.
- Ericson, T., Weise, W., 1988, *Pions and Nuclei*, Clarendon Press, Oxford, p. 175ff.
- Finley, J. P., Ögelman, H., 1993, IAU Circ., **No. 5787**.
- Finley, J. P., Ögelman, H., Kiziloglu, Ü., 1992, ApJ, **394**, L21.
- Finley, J. P., Ögelman, H., Hasinger, G., Trümper, J., 1993, ApJ, **410**, 323.

- Flowers, E., Sutherland, P., Bond J.R., 1975, Phys. Rev., **D12**, 315.
- Flowers, E., Ruderman, M., Sutherland, P., 1976, ApJ, **205**, 541.
- Friman, B., Maxwell, O. (FM79), 1979, ApJ, **232**, 541.
- Glendenning, N. K., 1985, ApJ, **293**, 470.
- Glendenning, N. K., 1989, Nucl. Phys., **A493**, 521.
- Gnedin, O., Yakovlev, D., 1995, Nucl. Phys., **A 582**, 697.
- Halpern, J., Ruderman, M., 1993, ApJ, **415**, 286.
- Haubold, H., Käempfer, B., Senatorov, A., Voskresensky, D., 1988, A&A, **191**, L22.
- Huber, H., Weber, F., Weigel, M. K., 1994, Phys. Rev., **C50**, R1287.
- Huber, H., Weber, F., Weigel, M. K., 1996, Nucl. Phys., **A 596**, 684.
- Itoh, N., 1983, ApJ, **273**, 774.
- Itoh, N., Kohyama, Y., 1983, ApJ, **275**, 859.
- Itoh, N., Kohyama, Y., Matsumoto, N., Seki, M., 1984, ApJ, **285**, 758.
- Itoh, N., Tomoo, A., Nakagawa, M., Kohyama, Y., 1989, ApJ, **339**, 354.
- Kolomeitsev, E., Voskresensky, D., Kämpfer, B., 1995, Nucl. Phys., **A588**, 889.
- Kunihiro, T., Takatsuka, T., Tamagaki, R., Tatsumi, T., 1993, Progress of Theoretical Physics, **112**, 123.
- Lattimer, J.M., Pethick, C.J., Prakash, M., Haensel, P., 1991, Phys. Rev. Lett., **66**, 2701.
- Maxwell, O., 1979, ApJ, **231**, 201.
- Maxwell, O., Brown, G., Campbell, D., Dashen, R., Manassah, J., 1977, ApJ, **216**, 77.
- Migdal, A. B., 1971, Zh. Eksp. Teor. Fiz., **61**, 2209, in Engl.: 1972, JETP, **34**, 1184.
- Migdal, A. B., 1978, Rev. Mod. Phys., **50**, 107.
- Migdal, A. B., Saperstein, E., Troitsky, M., Voskresensky, D., 1990, Phys. Rep., **192**, 179.
- Mitake, S., Ichimaru, S., Itoh, N., 1984, ApJ, **277**, 375.
- Muzikar, P., Sauls, J., Serene, J., 1980, Phys. Rev., **D21**, 1494.
- Negele, J., Vautherin, D., 1973, Nucl. Phys., **A 207**, 298.
- Ögelman, H., 1995, in *The Lives of the Neutron Stars*, edited by M. Alpar, Ü. Kiziloglu, J. van Paradijs, Kluwer, Dordrecht, p. 101.
- Ögelman, H., Finley, J.P., 1993, ApJ, **413**, L31.
- Ögelman, H., Finley, J.P., Zimmermann, H., 1993, Nature, **361**, 136.
- Page, D., 1995, Revista Mexicana de Física, **41** (Suplemento 1), 178.
- Pethick, C., Thorsson, V., 1994, Phys. Rev. Lett., **72**, 1964.
- Pethick, C., Ravenhall, P., Lorenz, C., 1995, Nucl. Phys., **A584**, 675.
- Prakash, M., Prakash, M., Lattimer, J.M., Pethick, C.J., 1992, ApJ, **390**, L77.
- Reisenegger, A., 1995, ApJ, **442**, 749.
- Richardson, M. B., Van Horn, H. M., Ratcliff, K. F., Malone, R. C., 1982, ApJ, **255**, 624.
- Safi-Harb, S., Ögelman, H., 1995, in *The Lives of the Neutron Stars*, edited by A. Alpar, Ü. Kiziloglu, J. van Paradijs, Kluwer, Dordrecht, p.53.
- Sawyer R.F., 1972, Phys. Rev. Lett. **29**, 382.

- Scalapino D.J., 1972, Phys. Rev. Lett. **29**, 386.
- Schaab, Ch., Weber, F., Weigel, M. K., Glendenning, N. K., 1996, Thermal evolution of compact stars, Nucl. Phys., **A605**, 531.
- Schaab, Ch., Sedrakian, A. D., Weber, F., Weigel, M. K., Internal Heating and Evolution of Neutron Stars, in preparation.
- Sedrakian, A. D., Sedrakian, D. M., 1993, ApJ, **413**, 658.
- Senatorov, A., Voskresensky, D., 1987, Phys. Lett., **B184**, 119.
- Seward, F., Wang, Z.-R., 1988, ApJ, **332**, 199.
- Seward, F., Harnden, F., Murdin, P., Clark, D., 1983, ApJ, **267**, 698.
- Shapiro, S. L., Teukolsky, S. A., 1983, *Black Holes, White Dwarfs and Neutron Stars*, John Wiley & Sons, p. 328.
- Shibazaki, N., Lamb, F. K., 1989, ApJ, **346**, 808.
- Takatsuka, T., Tamagaki, R., 1980, Progress of Theoretical Physics, **64**, 2270.
- Thorne, K., 1977, ApJ, **212**, 825.
- Thorsson, V., Prakash, M., Lattimer, J.M., 1994, Nucl. Phys., **A572**, 693.
- Thorsson, V., Prakash, M., Tatsumi, T., Pethick, C.J., 1995, Phys. Rev., **D52**, 3739.
- Trussoni, E., Brinkmann, W., Ögelman, H., Hasinger, G., Aschenbach, B., 1990, A&A, **234**, 403.
- Tsuruta, S., 1966, Canadian Journal of Physics, **44**, 1863.
- Tsuruta, S., Cameron, A.G.W., 1965, Canadian Journal of Physics, **43**, 2056.
- Umeda, H., Tsuruta, S., Nomoto, K., 1994, ApJ, **433**, 256.
- Van Riper, K. A., 1988, ApJ, **329**, 339.
- Van Riper, K. A., 1991, ApJ Suppl., **75**, 449.
- Van Riper, K. A., Link, B., Epstein, R. I., 1995, ApJ, **448**, 294.
- Voskresensky, D., Mishustin, I., 1978, Pisma v Zh. Eksp. Teor. Fiz., **28**, 486, in Engl.: 1978, JETP Lett., **28**, 449.
- Voskresensky, D., Mishustin, I., 1982, Yad. Fiz., **35**, 1139, in Engl.: 1982, Sov. J. Nucl. Phys., **35**, 667.
- Voskresensky, D., Senatorov, A. (VS84), 1984, Pisma v Zh. Eksp. Teor. Fiz., **40**, 395, in Engl.: 1984, JETP Lett., **40**, 1212.
- Voskresensky, D., Senatorov, A. (VS86), 1986, Zh. Eksp. Teor. Fiz., **90**, 1505, in Engl.: 1986, JETP, **63**, 885.
- Voskresensky, D., Senatorov, A., 1987, Yad. Fiz. **45**, 657, in Engl.: Sov. J. Nucl. Phys., **45**, 411.
- Voskresensky, D., Senatorov, A., Kämpfer, B., Haubold H., 1987, Astrophys. Space Sci. **138**, 421
- Wambach, J., Ainsworth, T., Pines, D., 1991, in *Neutron Stars: Theory and Observation*, edited by J. Ventura, D. Pines, pp. 37–48, Kluwer Academic Publishers, Dordrecht (Netherlands).

Weber, F., Weigel, M. K., 1989, Nucl. Phys., **A505**, 779.

Wiringa, R., Fiks, V., Fabrocini, A., 1988, Phys. Rev., **C38**, 1010.

Yancopoulos, S., Hamilton, T., Helfland, D., 1993, Bull. American Astron. Soc., **25**, 912.